

A Symmetrical Tetramer for *S. aureus* Pyruvate Carboxylase in Complex with Coenzyme A

Linda P.C. Yu,¹ Song Xiang,¹ Gorka Lasso,² David Gil,² Mikel Valle,² and Liang Tong^{1,*}

¹Department of Biological Sciences, Columbia University, New York, NY 10027, USA

²Structural Biology Unit, Center for Cooperative Research in Biosciences bioGUNE, 48160 Derio, Spain

*Correspondence: ltong@columbia.edu

DOI 10.1016/j.str.2009.04.008

SUMMARY

Pyruvate carboxylase (PC) is a conserved metabolic enzyme with important cellular functions. We report crystallographic and cryo-electron microscopy (EM) studies of *Staphylococcus aureus* PC (SaPC) in complex with acetyl-CoA, an allosteric activator, and mutagenesis, biochemical, and structural studies of the biotin binding site of its carboxyltransferase (CT) domain. The disease-causing A610T mutation abolishes catalytic activity by blocking biotin binding to the CT active site, and Thr908 might play a catalytic role in the CT reaction. The crystal structure of SaPC in complex with CoA reveals a symmetrical tetramer, with one CoA molecule bound to each monomer, and cryo-EM studies confirm the symmetrical nature of the tetramer. These observations are in sharp contrast to the highly asymmetrical tetramer of *Rhizobium etli* PC in complex with ethyl-CoA. Our structural information suggests that acetyl-CoA promotes a conformation for the dimer of the biotin carboxylase domain of PC that might be catalytically more competent.

INTRODUCTION

Pyruvate carboxylase (PC, EC 6.4.1.1) is a biotin-dependent enzyme and catalyzes the carboxylation of pyruvate to produce oxaloacetate (Attwood, 1995; Wallace et al., 1998; Jitrapakdee and Wallace, 1999; Jitrapakdee et al., 2006, 2008). PC is highly conserved and is found in most living organisms. In mammals, PC has crucial roles in gluconeogenesis, lipogenesis, glyceroneogenesis, insulin secretion, and other metabolic processes (Jitrapakdee and Wallace, 1999; Jitrapakdee et al., 2006, 2008). Inherited PC deficiencies are linked to serious diseases in humans such as lactic acidemia, hypoglycemia, psychomotor retardation, and death (Jitrapakdee and Wallace, 1999; Robinson, 2006). Four single-site mutations in PC, V145A, R451C, A610T, and M743I, have been associated with these diseases (Carbone et al., 1998; Wexler et al., 1998; Carbone and Robinson, 2003; Robinson, 2006).

In eukaryotes and most bacteria, PC is a single-chain enzyme of approximately 130 kDa in molecular weight, and is active only in its tetrameric form (Attwood et al., 1993, 1995; Jitrapakdee and Wallace, 1999; Jitrapakdee et al., 2008). In addition, the

activity of most PC enzymes is stimulated allosterically by acetyl-coenzyme A (acetyl-CoA) and inhibited by aspartate (Jitrapakdee and Wallace, 1999; Sueda et al., 2004; Jitrapakdee et al., 2007). Three domains were identified based on sequence comparisons with other biotin-dependent carboxylases (Cronan and Waldrop, 2002; Hall et al., 2004; Kondo et al., 2004; Tong, 2005; Studer et al., 2007). The biotin carboxylase (BC) domain at the N terminus catalyzes the first step of the reaction, the ATP- and Mg²⁺-dependent carboxylation of biotin, with bicarbonate as the carboxyl donor. The carboxyltransferase (CT) domain follows the BC domain in the primary sequence and catalyzes the transfer of the activated carboxyl group from carboxybiotin to pyruvate to form the oxaloacetate product (see Figure S1 available online). The active site of CT contains a tightly bound Mn²⁺ or Zn²⁺ divalent cation. The biotin cofactor is covalently linked to the side chain of a lysine residue in the biotin-carboxyl carrier protein (BCCP) domain, located at the C terminus of the enzyme.

Crystal structures of human, *S. aureus*, and *R. etli* PC (HsPC, SaPC, and RePC) have been reported recently by us and others (St. Maurice et al., 2007; Xiang and Tong, 2008). They reveal the organization of the tetramer (Figure 1A) and indicate that the BCCP domain must migrate between the BC active site of its own monomer and the CT active site of another monomer during catalysis, explaining why PC is only active in the tetrameric form. Interactions among the BC, CT, and a novel domain, the PC tetramerization (PT) domain, are important for the formation of this tetramer (Figure 1A). A generally symmetrical tetramer was observed for both HsPC and SaPC, although there are also significant differences in the relative positions of the BC and CT domains in the four monomers of SaPC (the HsPC structure is missing the BC domain) (Xiang and Tong, 2008). In contrast, a highly asymmetrical tetramer was observed for RePC, in complex with ethyl-CoA, an analog of the acetyl-CoA activator (St. Maurice et al., 2007). It was not clear whether this dramatic difference in the tetramer organization is truly due to the presence of ethyl-CoA, because the structures of HsPC and SaPC do not contain an activator. In addition, only the 3'-phospho-ADP portion of ethyl-CoA was ordered in the RePC structure, whereas the conformation of the rest of the CoA molecule was not observed.

In the structures of both HsPC and SaPC, a biotin coenzyme was captured in the active site of the CT domain (Figure 1B), providing the first molecular insight into how biotin could participate in the carboxyltransfer reaction (Xiang and Tong, 2008). The structures identify a collection of residues in the CT active site that might be important for catalysis, and most of them are highly

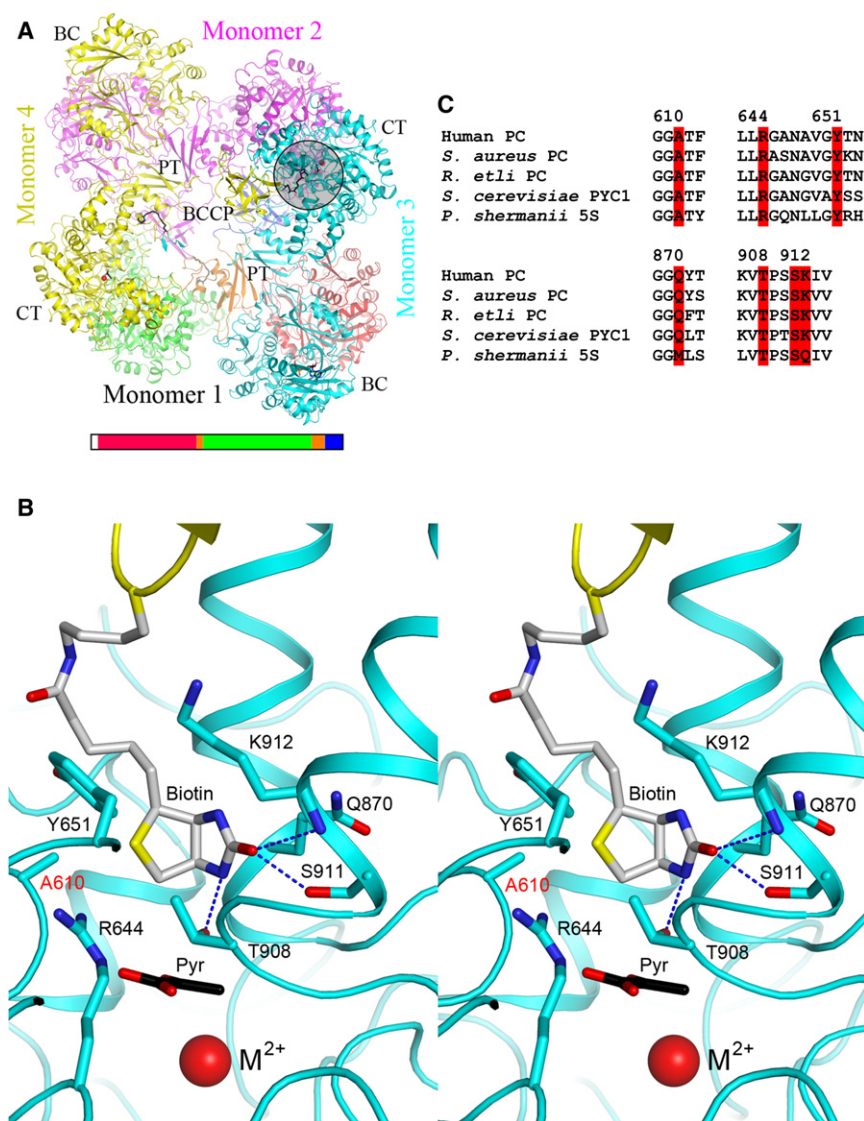


Figure 1. Structure of *S. Aureus* Pyruvate Carboxylase

(A) Schematic drawing of the structure of wild-type SaPC tetramer (Xiang and Tong, 2008), viewed from the bottom layer. The domains in monomer 1 are given separate colors: BC in red, CT in green, PT in gold, and BCCP in blue (also indicated in the bar graph at the bottom). The other three monomers are colored in magenta, cyan, and yellow. The biotin moiety is shown as a stick model in black. The gray circle highlights the active site of CT domain in monomer 3, with a bound BCCP-biotin from monomer 4.

(B) Stereo drawing of the active site of the CT domain in SaPC. The biotin moiety is shown in gray. The side chains of residues selected for mutagenesis are shown as stick models.

(C) Conservation of residues in the active site of CT. All the structure figures were produced with PyMOL (DeLano, 2002).

a symmetrical tetramer, which we have confirmed by cryo-EM studies. This is in sharp contrast to the highly asymmetrical tetramer of *R. etli* PC in complex with ethyl-CoA (St. Maurice et al., 2007).

RESULTS AND DISCUSSION

Selection of Residues in the CT Active Site for Mutagenesis

Based on a careful examination of the structure of SaPC, we identified 6 residues in the CT active site that might have important roles in biotin binding and/or catalysis: Ala610, Tyr651, Gln870, Thr908, Ser911, and Lys912 (Figure 1B). These residues are highly conserved among the PC enzymes (Figure 1C). (To simplify discussions, the residues in

conserved among the PC enzymes (Figure 1C). Two of the disease-causing mutations, A610T and M743I, are located in this active site (Hall et al., 2004; Xiang and Tong, 2008), although the functional importance of the other residues in the biotin binding site has not been characterized. The structure of SaPC also reveals an exo site for biotin binding (Xiang and Tong, 2008), which might exist in RePC as well (Jitrapakdee et al., 2008), but the functional role of this site is currently not known.

We report here structural and biochemical characterizations of SaPC carrying single-site mutations in the active site of the CT domain, as well as the structure of SaPC in complex with CoA. The studies demonstrate that the disease-causing A610T mutation abolishes catalytic activity by blocking biotin binding to the CT active site, and indicate that residue Thr908 might play a catalytic role in the CT reaction. Having structural information on SaPC in the absence and presence of CoA allowed us to carry out detailed structural comparisons to define conformational changes in the enzyme upon CoA binding. Surprisingly, our crystal structure showed that the CoA complex of SaPC is

SaPC and RePC are numbered according to their equivalents in HsPC.) Among these, Thr908 is hydrogen-bonded to the N1' atom and Ala610 is located near the sulfur atom of biotin (Figure 1B). Ser911 is hydrogen-bonded to the ureido oxygen of biotin. Gln870 is located near this oxygen atom, although it does not have direct interactions with the biotin. The side chains of Tyr651 and Lys912 have van der Waals interactions with biotin, contributing to the formation of its binding site. We have therefore designed the A610T, Y651A, Q870A, T908A, S911A, and K912T mutants. A610T corresponds to the disease-causing mutation, and the K912T mutation was selected as our modeling study suggests that the bulkier Thr side chain could disrupt the biotin binding site.

The other part of the CT active site, involved in the binding of the pyruvate substrate and the divalent cation, has previously been examined by mutagenesis studies in RePC (St. Maurice et al., 2007), the PC enzyme from *Bacillus thermodenitrificans* (Yong-Biao et al., 2004) and the CT (5S) subunit of the *Propionibacterium shermanii* transcarboxylase (Hall et al., 2004). The

disease-causing M743I mutation is located here and is expected to block binding of the pyruvate substrate (Hall et al., 2004). We have selected one residue in this area of the active site, Arg644, for mutagenesis. This residue is involved in a bi-dentate interaction with the pyruvate substrate in the structures of HsPC and SaPC (Figure 1B) (Xiang and Tong, 2008), but is pointed away from the substrate in the 5S structure (Hall et al., 2004). This residue is strictly conserved among the PC enzymes (Figure 1C). To examine the functional role of this residue in catalysis, we have generated the R644K and R644A mutants.

Mutations in the CT Active Site Can Greatly Reduce Catalytic Activity

The wild-type SaPC and the designed single-site mutants were overexpressed in *E. coli* and purified to homogeneity. The catalytic activity of the enzymes was assayed by monitoring the production of the oxaloacetate product at various pyruvate concentrations. The concentrations of the other substrates were kept at saturating levels in the assay, and the activator acetyl-CoA was not included in the reaction. The initial velocity data were fitted to the Michaelis-Menten equation (there was no indication of cooperative behavior) to obtain kinetic parameters for the wild-type enzyme and those mutants with sufficient catalytic activity (Table 1).

The kinetic data showed that two mutants, S911A and Q870A, maintained strong catalytic activity, with only a 1.5- and 2-fold loss in k_{cat}/K_m compared with the wild-type enzyme, respectively (Table 1). It is likely that the S911A mutation did not completely disrupt the interactions between the ureido oxygen atom of biotin and the enzyme, because this atom is also hydrogen-bonded to the main-chain amide of Lys912 (Figure 1B) (Xiang and Tong, 2008). The kinetic mechanism of PC catalysis suggests that the ureido oxygen might carry a negative charge during the CT reaction (Figure S1) (Attwood and Wallace, 2002; Jitrapakdee et al., 2008), and these interactions might be important for stabilizing this anionic intermediate.

The other mutants that we studied have greater than 30-fold loss in k_{cat} (Table 1), confirming the structural observations and the functional importance of these residues in the catalysis by PC. The data on the Arg644 mutants suggest that the bi-dentate interaction between this side chain and the pyruvate substrate is important for catalysis, in contrast to the structural observations on the 5S subunit of transcarboxylase (Hall et al., 2004). Our kinetic results on the A610T mutant of SaPC are consistent with those reported earlier on this mutant of HsPC (Carbone et al., 1998; Wexler et al., 1998; Carbone and Robinson, 2003). To provide further information on the molecular basis for the effects of these mutations on the catalytic activity, we have determined the crystal structures of the A610T and T908A mutants.

The A610T Mutation Blocks Biotin Binding to the CT Active Site

The crystal structure of the A610T mutant of SaPC has been determined at 2.9 Å resolution (Table 2). The overall organization of the tetramer of this mutant is similar to that of the wild-type enzyme (Figure 2A), with a root-mean-square (rms) distance of 0.67 Å among 4057 equivalent $C\alpha$ atoms of the two tetramers. However, the structure revealed that none of the biotin groups are present in the active site of the CT (or BC) domains. Instead,

Table 1. Summary of Kinetic Parameters

SaPC	K_m for Pyruvate (mM)	k_{cat} (s^{-1})	k_{cat}/K_m ($\text{mM}^{-1} \text{s}^{-1}$)
<i>Without acetyl-CoA</i>			
Wild-type	4.4 ± 0.5	6.5 ± 0.3	1.5 ± 0.2
S911A	2.3 ± 0.6	2.5 ± 0.2	1.1 ± 0.3
Q870A	1.8 ± 0.4	1.2 ± 0.1	0.7 ± 0.2
A610T	—	<0.1	—
T908A	—	<0.2	—
K912T	—	<0.2	—
Y651A	—	<0.1	—
R644K	—	<0.2	—
R644A	—	<0.2	—
<i>With acetyl-CoA</i>			
Wild-type	0.58 ± 0.04	15.7 ± 0.6	27.2 ± 2.3

The catalytic activity was determined following the appearance of oxaloacetate, which was coupled to NADH oxidation through malate dehydrogenase (Modak and Kelly, 1995). The concentration of the pyruvate substrate was varied in the reactions, while the concentrations of the other substrates were kept at saturating levels. The experiments were repeated several times to ensure reproducibility, and data from one representative assay are shown. Standard deviations were obtained from fitting the experimental data to the Michaelis-Menten equation.

all of them are located in the exo site (Xiang and Tong, 2008). Detailed inspection of the biotin binding site confirms the expectation that introduction of the bulkier Thr side chain in the mutant causes serious steric clashes with biotin (Figure 2B), thereby blocking its binding and involvement in catalysis. The distance between residue Ala610 and the sulfur atom of biotin is 4.1 Å. In the mutant, the distance would be reduced to 2.3 Å, much shorter than the allowed contact distance of 3.5 Å.

Coupled with the relocation of BCCP-biotin from the CT active site to the exo site, there is a large conformational change for the C-terminal segment (residues 863–983) of the CT domain in the A610T mutant structure (Figure 2C), so that it now resembles that of the free CT domain (Xiang and Tong, 2008). This provides further evidence that the C-terminal segment of CT must undergo a conformational change to accommodate BCCP-biotin in its active site (Xiang and Tong, 2008).

Residue Thr908 Might Have an Important Role in Catalysis

The crystal structure of the T908A mutant of SaPC has been determined at 2.7 Å resolution (Table 2). The overall structure of the mutant tetramer is essentially the same as the wild-type tetramer, with an rms distance of 0.55 Å for 4275 equivalent $C\alpha$ atoms between them. Moreover, one biotin is located in the CT active site whereas the other three are in the exo site, just like that in the wild-type enzyme. There are essentially no conformational differences in the biotin binding site between the wild-type and mutant (Figure 3D). The structural information therefore suggests that the hydrogen-bond between Thr908 and the N1' atom of biotin might not be essential for biotin binding in the CT active site. The fact that the T908A mutant has a > 30-fold loss in k_{cat} (Figure 2B) suggests that this residue might instead be important for catalysis by PC.

Table 2. Data Collection and Refinement Statistics

Structure	A610T Mutant	T908A Mutant	CoA Complex
Space group	$P2_1$	$P2_1$	$P2_12_12_1$
Cell dimensions			
<i>a</i> , <i>b</i> , <i>c</i> (Å)	96.6, 256.8, 126.5	96.5, 257.2, 130.3	96.6, 164.5, 373.3
α , β , γ (°)	90, 109.6, 90	90, 114.4, 90	90, 90, 90
Resolution (Å)	30-2.9 (3.0-2.9)	30-2.7 (2.8-2.7)	30-2.9 (3.0-2.9)
R_{merge} (%)	7.5 (42.2)	8.7 (43.7)	13.9 (47.8)
$I / \sigma I$	12.2 (2.5)	10.8 (2.7)	8.7 (3.2)
Completeness (%)	93 (84)	87 (78)	96 (100)
Redundancy	2.6 (2.5)	3.0 (3.1)	6.9 (4.7)
Number of reflections	112,542	128,213	112,448
R_{work} (%)	22.0 (30.5)	22.8 (32.6)	26.4 (28.6)
R_{free} (%)	26.6 (37.4)	28.0 (39.8)	32.8 (41.3)
Rms deviations			
Bond lengths (Å)	0.006	0.007	0.009
Bond angles (°)	1.0	1.1	1.3

The numbers in parentheses are for the highest-resolution shell. One crystal was used for each data collection.

Our structural analysis suggests that Thr908 could serve as a general acid/general base during the CT reaction. In fact, a general base is needed to extract a proton from the methyl group of pyruvate and a general acid is needed to protonate the N1'

atom of biotin in the forward direction of the CT reaction (Figure S1) (Attwood and Wallace, 2002; Jitrapakdee et al., 2008). The side-chain hydroxyl group of Thr908 could serve both of these functions, because it is hydrogen-bonded to the

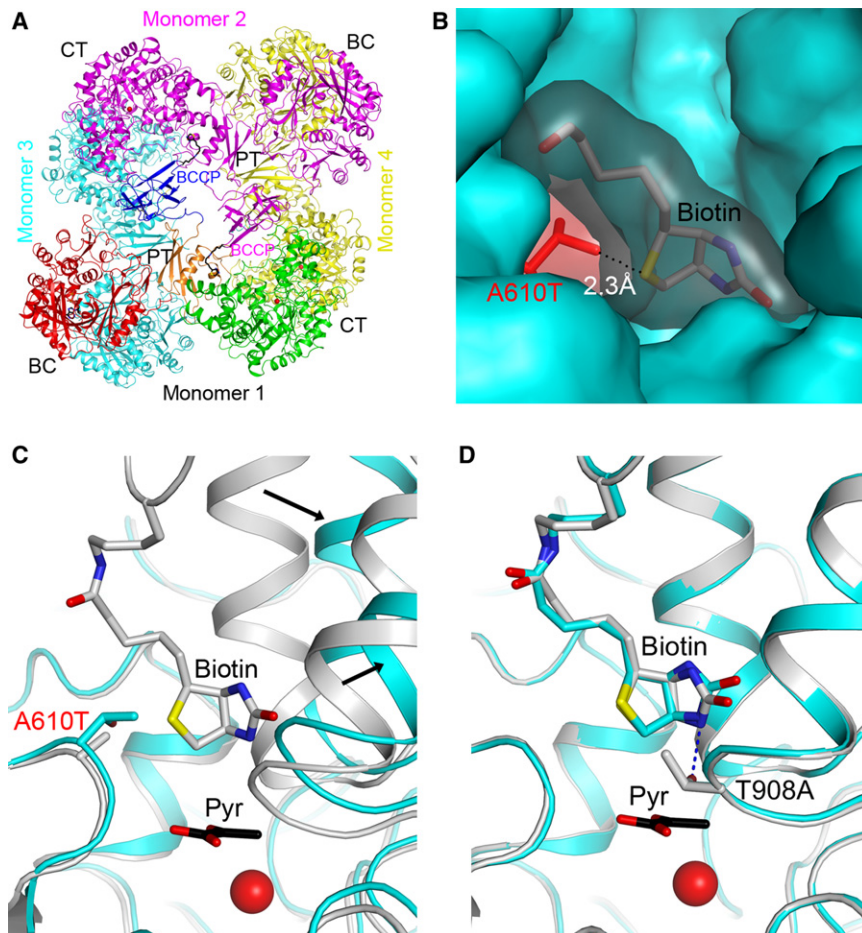


Figure 2. Structures of the A610T and T908A Mutants of SaPC

(A) Schematic drawing of the tetramer of the A610T mutant of SaPC, viewed from the top layer and colored as in Figure 1A.

(B) Molecular surface of the A610T mutant showing the steric clash between the Thr610 residue and the bound position of biotin as observed in the wild-type structure.

(C) Schematic drawing showing the overlay of the biotin binding site in the A610T mutant (in color) and the wild-type enzyme (in gray). Large conformational differences for the C-terminal segment of CT are visible, associated with the relocation of biotin to the exo site in the mutant structure. The bound position of pyruvate (in black) as observed in the wild-type SaPC structure is also shown.

(D) Schematic drawing showing the overlay of the biotin binding site in the T908A mutant (in color) and the wild-type enzyme (in gray).

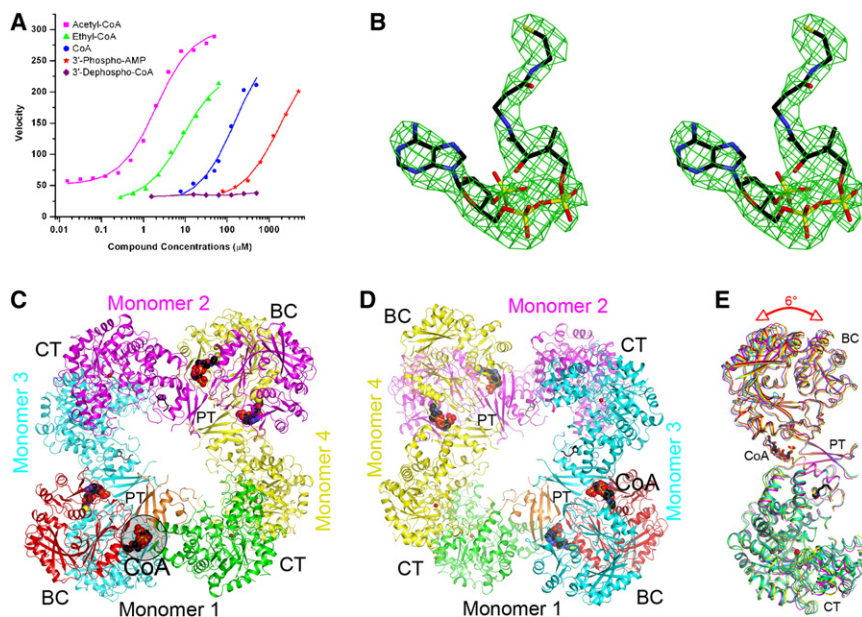


Figure 3. A Symmetrical Tetramer for SaPC in Complex with CoA

(A) Activation of SaPC catalysis by various acetyl-CoA analogs. A representative titration for each compound is shown.

(B) Omit $F_o - F_c$ electron density at 2.9 Å resolution for CoA. The contour level is at 3σ .

(C) Schematic drawing of the tetramer of the CoA complex of SaPC, colored as in Figure 1A. The CoA molecules are shown as space-filling models in black. One binding site for CoA is highlighted with the gray circle.

(D) Schematic drawing of the tetramer of the CoA complex of SaPC, viewed from the bottom layer.

(E) Overlay of the structures of the four monomers of SaPC in the CoA complex, based on their CT domains. The BC domains show a 6° difference in their relative orientations.

N1' atom of biotin and is about 4 Å away from the methyl group of pyruvate in the structure (Figure 1B). The pK_a value of this hydroxyl group might be in the same range as that for the N1' atom of biotin and the methyl group of pyruvate (after enolization through binding to the divalent cation).

The structures of both the A610T and the T908A mutants reported here are in the free enzyme state, whereas that of the wild-type enzyme was in complex with the substrate pyruvate (Xiang and Tong, 2008). Because biotin was found in the active site in the T908A mutant, in the same conformation as observed in the wild-type SaPC, it is unlikely that pyruvate binding is needed to facilitate binding of biotin to the CT active site.

Interestingly, we have so far not observed the binding of BCCP-biotin to the BC active site in the structures reported here and in the structure of wild-type SaPC reported earlier (Xiang and Tong, 2008). It might be possible that BCCP-biotin has higher affinity for the CT active site and the exo site under the experimental conditions that we have used. Further studies are needed to identify conditions that will favor the binding of BCCP-biotin to the active site of the BC domain.

A Symmetrical Tetramer for SaPC in Complex with CoA

To provide further biochemical data on the interactions between acetyl-CoA and PC, we characterized the activating effect of a series of acetyl-CoA analogs on the catalysis by SaPC. The concentration of the pyruvate substrate was kept near its K_m (5 mM, Table 1) while the other substrates were present at saturating levels in the kinetic experiments. The data showed that acetyl-CoA is the most potent at activating SaPC, with a K_a of $2.0 \pm 0.3 \mu\text{M}$, whereas the K_a for ethyl-CoA is $8.7 \pm 1.0 \mu\text{M}$ (Figure 3A). In comparison, the K_a values of these two compounds for RePC are 30 and 360 μM (St. Maurice et al., 2007). Removal of the acetyl group led to an 80-fold loss in activation, as the K_a for CoA is $160 \pm 60 \mu\text{M}$. In the structure of RePC, only the 3'-phospho-ADP portion of ethyl-CoA is ordered (St. Maurice et al., 2007). The closest commercially available analog of this

compound is 3'-phospho-AMP (or adenosine 3',5'-bisphosphate), which has a K_a of $1800 \pm 270 \mu\text{M}$ (Figure 3A), suggesting that the β -mercaptoethylamine and the pantotheine groups of CoA might also be beneficial for PC activation. The most important group on acetyl-CoA for activating PC appears to be the 3' phosphate, because 3'-dephospho-CoA had no effect on PC even at 0.5 mM concentration (Figure 3A).

Further kinetic studies showed that acetyl-CoA gives rise to both an increase in the k_{cat} of SaPC and a decrease in its K_m for the pyruvate substrate, such that the overall k_{cat}/K_m is increased 18-fold in the presence of saturating (100 μM) acetyl-CoA (Table 1). The initial velocity data appear to obey Michaelis-Menten kinetics, with no sign of cooperativity (data not shown). Our kinetic data on acetyl-CoA activation of SaPC are consistent with those reported for other PC enzymes sensitive to this compound (Attwood and Wallace, 1986; Branson et al., 2002; St. Maurice et al., 2007; Jitrapakdee et al., 2008).

To reveal the conformational changes in SaPC upon acetyl-CoA activation, we determined the crystal structure of the enzyme in complex with CoA at 2.9 Å resolution (Table 2). The relatively higher R values for the diffraction data and the atomic model are due to the long c axis of the crystal (373 Å), which caused substantial overlaps among the diffraction spots. This was the best diffraction data set that we collected after screening through many crystals. The crystals were grown in the presence of acetyl-CoA, but only electron density for CoA was observed from the crystallographic analysis (Figure 3B). The acetyl group was either hydrolyzed during crystallization or disordered in the crystal. In fact, it has been reported that some PC enzymes can hydrolyze acetyl-CoA (Frey and Utter, 1977; Chapman-Smith et al., 1991). Nonetheless, the binding modes of the pantotheine and the β -mercaptoethylamine groups of CoA are clearly defined by the structure. All four BCCP domains are disordered in the structure, although weak electron density was observed for two biotin groups in the exo site, one in each layer of the structure (Figure 3C).

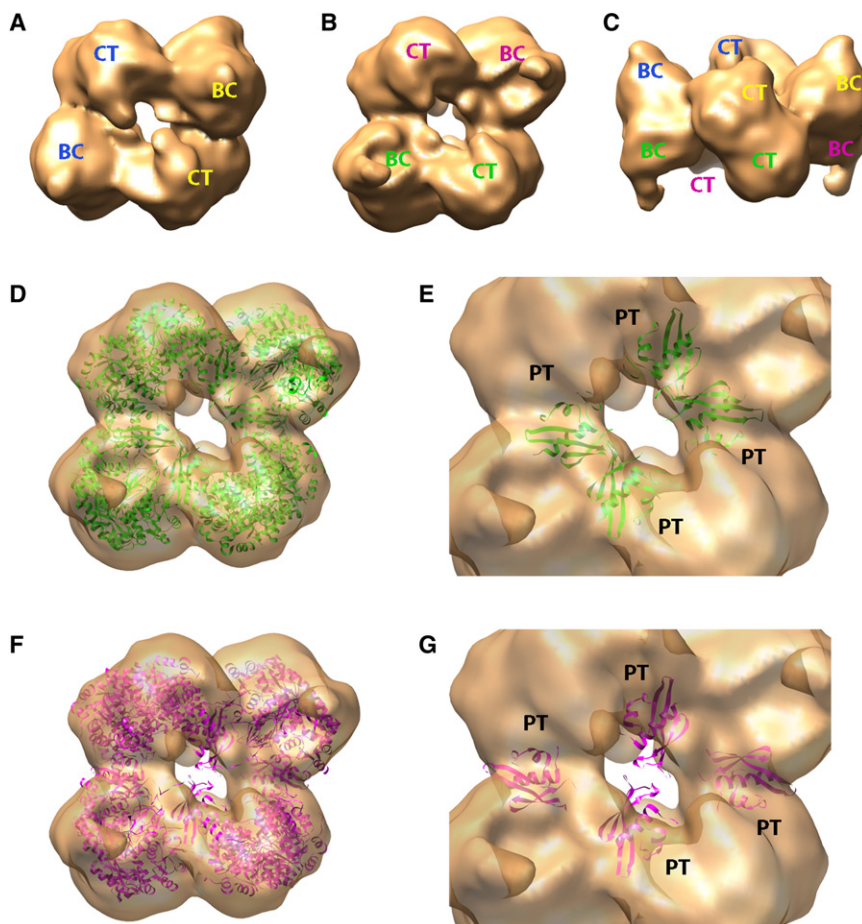


Figure 4. Cryo-EM Studies Confirm a Symmetrical Tetramer for SaPC in Complex with Acetyl-CoA

(A–C) The cryo-EM density of SaPC in the presence of acetyl-CoA: top view (A), bottom view (B), and side view (C).

(D) Fit of the symmetrical tetramer of SaPC in complex with CoA into the cryo-EM map. The atomic model is colored in green.

(E) Close-up showing the fit between the PT domains of SaPC and the cryo-EM map.

(F) The asymmetrical tetramer of RePC cannot be completely accommodated into the cryo-EM map.

(G) Close-up showing the PT domains of RePC lying outside the cryo-EM envelope.

discontinuous density is observed for the four B domains of BC, and they are not included in the current atomic model (Figure 3C). As a result, there are no adenine nucleotides in the BC active sites in this structure.

Cryo-EM Studies Confirm a Symmetrical Tetramer in the Presence of Acetyl-CoA

To obtain direct, independent evidence for the symmetrical tetramer for the CoA complex observed in our crystal structure, we next carried out cryo-EM studies on SaPC. Consistent with earlier observations on chicken liver PC (Attwood et al., 1993), the SaPC tetramer is not

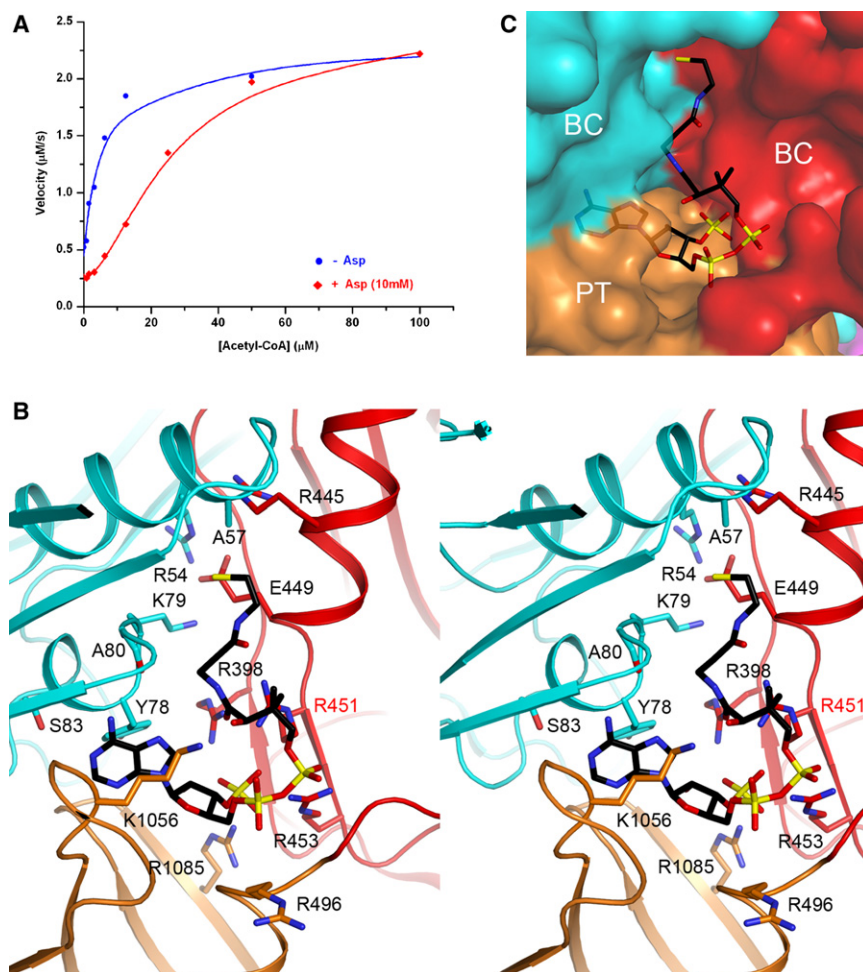
In sharp contrast to the asymmetrical RePC structure, the structure of SaPC in complex with CoA is symmetrical, with a CoA molecule bound to each monomer of the tetramer (Figures 3C and 3D). In fact, the structure in complex with CoA is even more symmetrical than that in the absence of CoA. The four monomers of SaPC in the absence of CoA have large differences in the relative positions of their BC and CT domains (Xiang and Tong, 2008). When the CT domains of the four monomers are superimposed, a 6°–18° difference is seen in the relative orientations of the four BC domains. In contrast, for the structure in complex with CoA, the difference in the relative orientations of the four BC domains is only 6° (Figure 3E). This shows that the domain organization of the four monomers has become more similar to each other and the tetramer has become more symmetrical in the CoA complex. The rms distance between equivalent C α atoms for any pairs of the domains in the CoA complex is 0.6 Å.

The asymmetrical RePC structure possesses a single two-fold axis of symmetry, relating the two monomers in the same layer of the tetramer. In comparison, the structure of the CoA complex of SaPC possesses nearly 222 symmetry, which also relates monomers in the different layers of the tetramer. The presence of only two copies of biotin, in the exo site on different layers, represents a deviation from this 222 symmetry. The significance of this deviation remains to be determined, because all four BCCP domains are disordered in the current crystal. In addition, only very weak,

very stable at low concentrations in the absence of acetyl-CoA, which hindered the three-dimensional averaging for this state of the enzyme. In contrast, the PC tetramer is much more stable in the presence of acetyl-CoA, allowing the production of a cryo-EM model at roughly 13 Å resolution, which clearly resembles the overall features of the PC tetramer observed in the crystal structure (Figures 4A–4C).

Although only two-fold symmetry was enforced during the three-dimensional averaging, the cryo-EM map is remarkably symmetrical, consistent with overall 222 symmetry for the tetramer (Figures 4A–4C). In fact, our crystal structure of the CoA complex of SaPC could be readily fit into the cryo-EM map (Figure 4D), with all the structural features located within the boundaries of the cryo-EM envelope (Figure 4E). In contrast, the asymmetrical tetramer of RePC could not be completely accommodated within the cryo-EM model (Figure 4F), and the discrepancy is especially obvious for the PT domains (Figure 4G). We did not observe any evidence for an asymmetrical tetramer for SaPC from the cryo-EM studies. Overall, the cryo-EM data provide clear evidence that SaPC in solution forms a symmetrical tetramer in the presence of acetyl-CoA, confirming our observations in the crystal structure.

A symmetrical PC tetramer is consistent with biochemical data. Studies of chicken liver PC showed that four acetyl-CoA molecules can bind to each tetramer, with apparent positive cooperativity (Hill coefficient of 1.9) (Frey and Utter, 1977).

**Figure 5. Binding Mode of CoA in SaPC**

(A) SaPC displays positive cooperativity toward acetyl-CoA binding in the presence of aspartate. (B) Detailed interactions between CoA and the BC and PT domains in the complex with SaPC. The CoA molecule is shown in black. (C) Molecular surface of SaPC near the CoA binding site, colored as in (B).

group is surrounded by a cluster of four Arg side chains, Arg398, Arg451, and Arg453 from the BC domain, and Arg1085 from the PT domain, explaining its importance for binding (Figure 3A). R451C is one of the disease-causing mutations, and our earlier kinetic studies have shown that this mutant is much less sensitive to acetyl-CoA activation (Xiang and Tong, 2008). The α - and β -phosphates of CoA interact with the side chain of Arg453 and the main-chain amides of residues 495–497, at the hinge region between the BC and PT domains (Figure 5B).

The rest of the CoA molecule follows the interface of the BC dimer (Figure 5C), having mostly van der Waals interactions with the enzyme. The thiol group of CoA is located in a small depression in the surface of the dimer, surrounded by the side chains of Arg54', Ala57', Lys79', Arg445, and Glu449 in the two BC domains (Figure 5B). Residues Arg54, Lys79, and Arg445 are strictly conserved

Studies of acetyl-CoA activation of yeast PC also demonstrated positive cooperativity, with a Hill coefficient of 2, but only in the presence of the *L*-aspartate inhibitor (Cazzulo and Stoppani, 1968; Jitrapakdee et al., 2007). SaPC behaves similarly to the yeast enzyme, with the cooperative behavior (Hill coefficient of 2) being manifested only in the presence of aspartate (Figure 5A). Although further studies are needed to define the exact binding site for aspartate, the kinetic data showed that the inhibitory effect of this compound could be overcome at high concentrations of acetyl-CoA (Figure 5A). This suggests that the conformation of PC in complex with acetyl-CoA might not allow aspartate binding.

Binding Mode of CoA

Our structure showed that the 3'-phospho-ADP portion of CoA is bound at the interface between the BC-PT domains of one monomer and the BC domain of another monomer (Figure 5B). The adenine base is buried in a small pocket on the surface of the enzyme (Figure 5B), flanked by the side chain of Lys1056 in the PT domain and the main chain of Tyr78' in the BC domain (with the prime indicating the other monomer). The N6 atom of adenine is hydrogen-bonded to the main-chain carbonyl oxygen of Ala80', and the N1 atom is located near the side chain of Ser83', although this residue is not conserved. The 3'-phosphate

among the single-chain PC enzymes. Moreover, Arg54 is also conserved in the BC subunit of *E. coli* acetyl-CoA carboxylase, which shares a similar mode of dimerization. Mutation of this equivalent residue in *E. coli* BC, Arg19, to Glu can disrupt the dimer of that enzyme, and the monomeric form of this mutant has a 3-fold loss in catalytic activity (Shen et al., 2006). This suggests that one function of acetyl-CoA binding might be to stabilize the dimer of BC domains, consistent with our observation in the cryo-EM studies that the SaPC tetramer is much less stable in the absence of acetyl-CoA and earlier studies with the chicken liver PC (Attwood et al., 1993). Half-of-the-sites reactivity has been proposed for the *E. coli* BC dimer (Janiyani et al., 2001; de Queiroz and Waldrop, 2007; Mochalkin et al., 2008), although the substrate complex of BC is fully symmetrical (Chou et al., 2009) and monomeric mutants of the enzyme are catalytically active (Shen et al., 2006).

Molecular Basis for Activation of PC by Acetyl-CoA

Based on the asymmetrical tetramer of RePC, it was suggested that acetyl-CoA stimulates PC activity by reducing the distances between the BC and CT active sites (St. Maurice et al., 2007). However, in the symmetrical tetramer of the CoA complex of SaPC (Figure 4D), the distances between the BC and CT active sites are essentially the same as those in the free enzyme,

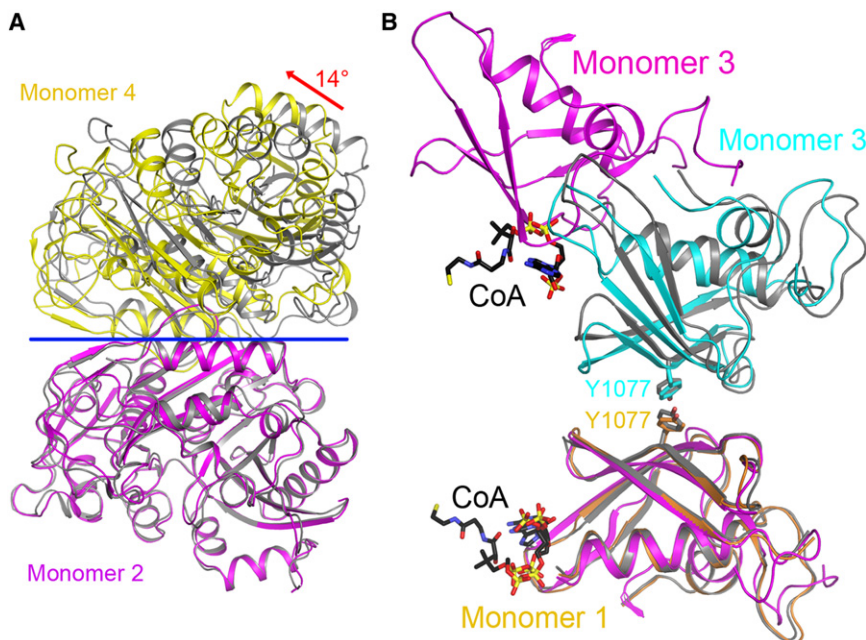


Figure 6. Conformational Changes in SaPC upon CoA Binding

(A) Overlay of the structure of the BC domain dimer in the CoA complex (in color) and free enzyme (in gray) of SaPC. The structure of one monomer is overlaid, showing a large difference in the positions of the other monomer. The two-fold axis of the dimer is indicated by the horizontal line in blue. (B) Overlay of the PT domain dimers in the CoA complex (in color) and free enzyme (in gray) of SaPC, as well as the two equivalent PT domains in RePC (in magenta).

roughly 75 Å (Xiang and Tong, 2008). Therefore, this mechanism of activation is unlikely to apply to SaPC.

Detailed comparisons between the structures of SaPC in the absence and presence of CoA show that the organization of the BC dimers has large differences between the two tetramers (Figure 6A), whereas the organization of the CT dimers is not affected by CoA binding (data not shown). With one monomer of the BC dimer in overlay, the other monomers of the dimer show a difference of 14° in their orientations. A reorganization of the BC dimer is consistent with the binding of CoA to its interface and with earlier biochemical data showing that acetyl-CoA primarily affects the BC reaction (Jitrapakdee et al., 2008). Therefore, the structural and biochemical data suggest that acetyl-CoA might promote and stabilize an organization of the BC domain dimer that is catalytically more competent. Studies with *E. coli* BC showed that changes in the dimer interface could affect catalysis in the active site (Shen et al., 2006), suggesting long-range communication between the two regions (Janiyani et al., 2001; de Queiroz and Waldrop, 2007; Mochalkin et al., 2008). The activation of PC by acetyl-CoA might involve a similar mechanism, although further studies are needed to characterize the molecular details of this communication.

Our structure is for the CoA complex of SaPC, although acetyl-CoA is 80-fold more potent at stimulating this enzyme than CoA (Figure 3A). It is possible that the acetyl group could enhance the interactions with the binding site in the BC dimer interface, and the negative charge on the sulfur atom of CoA might also be detrimental for the stimulatory effect. In addition, the current structure does not contain any substrates in the active sites (Figure 5B), which could also affect the stimulation by acetyl-CoA.

The structural comparisons show that CoA binding and the reorganization of the BC domain dimer also caused a change in the PT dimer of SaPC (Figure 6B), although the PT domain remains in the tetramer interface and residue Tyr1077 is still

located in the center of the PT dimer interface in this complex (Figure 3C). Our earlier kinetic data showed that the Y1077A mutant of SaPC is catalytically inactive in the absence of acetyl-CoA, but could be rescued by the presence of 0.5 mM acetyl-CoA (Xiang and Tong, 2008). These data suggest that acetyl-CoA binding stabilizes the BC domain dimer such that a mutation in the PT domain can be tolerated. The Tyr1077 residue contributes roughly 70 Å² of the 350 Å² surface area buried at the PT dimer interface. A much higher concentration of acetyl-CoA is needed to rescue the Y1077A mutant (K_a of 120 μM) than to activate the wild-type enzyme (K_a of 2 μM), demonstrating that the PT domain still has an important contribution to the stability of the SaPC tetramer in complex with CoA.

Comparison with the Structure of *R. etli* PC

The largest structural difference between the RePC tetramer and the CoA complex of SaPC is the organization of the PT domains (Figure 6B). Although a dimeric association is observed in SaPC, the two PT domains (called the allosteric domains) in RePC show essentially no interactions with each other (Figure 6B) and are exposed to the solvent (St. Maurice et al., 2007). However, the organizations of the BC and CT dimers of RePC are generally similar to those of SaPC. Therefore, the asymmetry of the RePC tetramer is due primarily to the large change in the PT domains.

The bound position of 3'-phospho-ADP in RePC relative to the PT domain is similar to that seen in the CoA complex of SaPC (Figure 6B). However, the adenine base is located farther away from the BC dimer interface in the RePC structure (Figure S2). In the two monomers of RePC that do not have this compound, the PT domain occupies the binding site for the adenine base, due to the large conformational change in this domain (Figure S2), suggesting that the conformation observed for RePC is incompatible with the binding of four acetyl-CoA molecules.

In summary, our structural studies have revealed a symmetrical tetramer for SaPC in complex with CoA, which is supported by biochemical data. Acetyl-CoA might activate PC by stabilizing the BC dimer and promoting a conformation of the tetramer that is more catalytically competent. Mutagenesis, kinetic, and structural studies have shown that Thr908 might play a catalytic role in the CT reaction of PC.

EXPERIMENTAL PROCEDURES

Protein Expression and Purification

Staphylococcus aureus PC (SaPC, residues 20–1178) was subcloned into vector pET28a (Novagen) and then overexpressed with a compatible plasmid that carries the bacterial biotin ligase (*birA*) gene in *E. coli* BL21Star cells, as reported earlier (Xiang and Tong, 2008). SaPC was purified by nickel-agarose affinity (QIAGEN) and gel-filtration (S-300, GE Healthcare) chromatography, concentrated to 10 mg/ml, flash-frozen in liquid nitrogen, and stored at -80°C in a buffer containing 20 mM Tris (pH 7.5), 200 mM NaCl, 2 mM DTT, and 5% (v/v) glycerol. An avidin binding gel-shift assay confirmed that the protein was fully biotinylated (data not shown).

Mutagenesis and Activity Assays

All mutants were made with the QuikChange Kit (Stratagene) and verified by sequencing. The mutant proteins were expressed and purified following the same protocol as that for the wild-type protein.

The catalytic activity of wild-type and mutant SaPC was determined at room temperature following the appearance of oxaloacetate, which was coupled to NADH oxidation through malate dehydrogenase (Modak and Kelly, 1995). The reaction mixture contained 100 mM Tris (pH 7.5), 200 mM NaCl, 5 mM MgCl_2 , 2 mM ATP, 50 mM sodium bicarbonate, varying concentrations of pyruvate, 0.2 mM NADH, 0.1 μM SaPC, and 10 U malate dehydrogenase (Sigma).

The effect of acetyl-CoA and various analogs on the catalytic activity of wild-type SaPC was determined by running the reactions in the presence of 5 mM pyruvate and varying concentrations of the compounds.

Protein Crystallization

Wild-type and mutant SaPC proteins were crystallized under similar conditions using the sitting-drop vapor diffusion method. The reservoir solution consisted of 20% (w/v) PEG3350 and 200 mM ammonium tartrate. For the mutants, 5 mM ATP was added to the protein solution. For the acetyl-CoA complex, 5 mM acetyl-CoA and 5 mM ATP were added to wild-type protein solution. All crystals grew within 1–3 days at room temperature. Cryoprotection was achieved by transferring the crystals to a 5 μl drop consisting of the reservoir solution supplemented with 20% (v/v) ethylene glycol.

Crystals of the A610T and T908A mutants are isomorphous to those of wild-type SaPC (Xiang and Tong, 2008) and there is a tetramer in the asymmetric unit. Crystals of wild-type SaPC grown in the presence of acetyl-CoA are in a new crystal form. There is a tetramer in the asymmetric unit.

Data Collection and Structure Determination

X-ray diffraction data were collected at the National Synchrotron Light Source (NSLS) beamlines X4A and X4C. The diffraction images were processed with the program HKL (Otwinowski and Minor, 1997), and the data processing statistics are summarized in Table 2. The crystal grown in the presence of acetyl-CoA had a long *c* axis (373 Å) and a relatively long *b* axis (164 Å), which produced substantial lunar overlaps among the diffraction spots. A lower mosaicity value had to be used during data processing to alleviate this overlap problem, which reduced the quality of the data set and the refinement statistics (Table 2). This was the best diffraction data set that was collected after screening through many crystals.

The structures were solved by molecular replacement using the wild-type SaPC structure as the search model with the program COMO (Jogl et al., 2001). Due to large conformational differences, the structure of the CoA complex was determined only when the individual domains of the monomer were used as the search models in the molecular replacement calculations. Manual rebuilding of the atomic models was carried out using O (Jones et al., 1991) and Coot (Emsley and Cowtan, 2004), and the structure refinement was accomplished with CNS (Brunger et al., 1998) and Refmac (Murshudov et al., 1997), with translation/libration/screw refinement. The refinement statistics are summarized in Table 2. The atomic coordinates have been deposited in the Protein Data Bank (accession numbers 3HB9, 3HBL, and 3HO8).

Electron Microscopy and Image Processing

SaPC at a concentration of 0.1 mg/ml in a buffer containing 20 mM Tris (pH 7.5), 2 mM NaCl, and 2 mM DTT was incubated with 2 mM acetyl-CoA for 20 min. Cryo-EM grids were prepared following standard procedures and

vitriified samples were examined on a JEM-2200FS/CR transmission electron microscope (JEOL Europe, Croissy-sur-Seine, France) at an acceleration voltage of 200 kV. Micrographs were taken on Kodak films under low-dose conditions at a magnification of 50,000, and were digitized on a Z/I Photoscan (ZEIS) scanner obtaining a final pixel size of 2.82 Å/pixel.

Particles were manually selected in the digitized micrographs and matched to particular reference-based projections. A three-dimensional reconstruction was performed using the Spire-spider package (Frank et al., 1996; Baxter et al., 2007), imposing two-fold (*C*₂) symmetry. In the calculation of the final 3D density map, a data set of 22,258 individual images was used. Resolution of the cryo-EM density map was estimated using a cutoff of 0.15 in the Fourier shell correlation (Rosenthal and Henderson, 2003). The atomic coordinates for PC were rigidly fitted into the reconstructed cryo-EM map using Chimera (Pettersen et al., 2004), which was also used to produce figures rendering cryo-EM maps.

SUPPLEMENTAL DATA

Supplemental Data include two figures and are available with this article online at [http://www.cell.com/structure/supplemental/S0969-2126\(09\)00189-0](http://www.cell.com/structure/supplemental/S0969-2126(09)00189-0).

ACKNOWLEDGMENTS

We thank Randy Abramowitz and John Schwanof for setting up the X4A and X4C beamlines at the NSLS, Melisa Lázaro for assistance during cryo-EM image processing, C. Huang for careful reading of the manuscript, and W. W. Cleland for helpful discussions. This research is supported in part by a grant from the National Institutes of Health (DK067238, to L.T.), the Etorrek Research Programmes 2007/2009 (Department of Industry, Tourism and Trade of the Government of the Autonomous Community of the Basque Country), and by the Innovation Technology Department of the Bizkaia County (to M.V.).

Received: January 26, 2009

Revised: March 31, 2009

Accepted: April 7, 2009

Published: June 9, 2009

REFERENCES

- Attwood, P.V. (1995). The structure and the mechanism of action of pyruvate carboxylase. *Int. J. Biochem. Cell Biol.* 27, 231–249.
- Attwood, P.V., and Wallace, J.C. (1986). The carboxybiotin complex of chicken liver pyruvate carboxylase. A kinetic analysis of the effects of acetyl-CoA, Mg^{2+} ions and temperature on its stability and on its reaction with 2-oxobutyrate. *Biochem. J.* 235, 359–364.
- Attwood, P.V., and Wallace, J.C. (2002). Chemical and catalytic mechanisms of carboxyl transfer reactions in biotin-dependent enzymes. *Acc. Chem. Res.* 35, 113–120.
- Attwood, P.V., Johannssen, W., Chapman-Smith, A., and Wallace, J.C. (1993). The existence of multiple tetrameric conformers of chicken liver pyruvate carboxylase and their roles in dilution inactivation. *Biochem. J.* 290, 583–590.
- Baxter, W.T., Leith, A., and Frank, J. (2007). SPIRE: the SPIDER reconstruction engine. *J. Struct. Biol.* 157, 56–63.
- Branson, J.P., Nezik, M., Wallace, J.C., and Attwood, P.V. (2002). Kinetic characterization of yeast pyruvate carboxylase isozyme pyc1. *Biochemistry* 41, 4459–4466.
- Brunger, A.T., Adams, P.D., Clore, G.M., DeLano, W.L., Gros, P., Grosse-Kunstleve, R.W., Jiang, J.-S., Kuszewski, J., Nilges, M., Pannu, N.S., et al. (1998). Crystallography & nmr system: A new software suite for macromolecular structure determination. *Acta Crystallogr. D Biol. Crystallogr.* 54, 905–921.
- Carbone, M.A., and Robinson, B.H. (2003). Expression and characterization of a human pyruvate carboxylase variant by retroviral gene transfer. *Biochem. J.* 370, 275–282.
- Carbone, M.A., MacKay, N., Ling, M., Cole, D.E.C., Douglas, C., Rigat, B., Feigenbaum, A., Clarke, J.T.R., Haworth, J.C., Greenberg, C.R., et al. (1998).

- Amerindian pyruvate carboxylase deficiency is associated with two distinct missense mutations. *Am. J. Hum. Genet.* **62**, 1312–1319.
- Cazzulo, J.J., and Stoppani, A.O.M. (1968). The regulation of yeast pyruvate carboxylase by acetyl-coenzyme A and L-aspartate. *Arch. Biochem. Biophys.* **127**, 563–567.
- Chapman-Smith, A., Booker, G.W., Clements, P.R., Wallace, J.C., and Keech, D.B. (1991). Further studies on the localization of the reactive lysyl residue of pyruvate carboxylase. *Biochem. J.* **276**, 759–764.
- Chou, C.-Y., Yu, L.P.C., and Tong, L. (2009). Crystal structure of biotin carboxylase in complex with substrates and implications for its catalytic mechanism. *J. Biol. Chem.* **284**, 11690–11697.
- Cronan, J.E., Jr., and Waldrop, G.L. (2002). Multi-subunit acetyl-CoA carboxylases. *Prog. Lipid Res.* **41**, 407–435.
- de Queiroz, M.S., and Waldrop, G.L. (2007). Modeling and numerical simulation of biotin carboxylase kinetics: implications for half-sites reactivity. *J. Theor. Biol.* **246**, 167–175.
- DeLano, W.L. (2002). *The Pymol Manual* (San Carlos, CA: DeLano Scientific).
- Emsley, P., and Cowtan, K.D. (2004). Coot: model-building tools for molecular graphics. *Acta Crystallogr. D Biol. Crystallogr.* **60**, 2126–2132.
- Frank, J., Radermacher, M., Penczek, P., Zhu, J., Li, Y., Ladjadi, M., and Leith, A. (1996). SPIDER and WEB: processing and visualization of images in 3D electron microscopy and related fields. *J. Struct. Biol.* **116**, 190–199.
- Frey, W.H., II, and Utter, M.F. (1977). Binding of acetyl-CoA to chicken liver pyruvate carboxylase. *J. Biol. Chem.* **252**, 51–56.
- Hall, P.R., Zheng, R., Antony, L., Pustai-Carey, M., Carey, P.R., and Yee, V.C. (2004). Transcarboxylase 5S structures: assembly and catalytic mechanism of a multienzyme complex subunit. *EMBO J.* **23**, 3621–3631.
- Janiyani, K., Bordelon, T., Waldrop, G.L., and Cronan, J.E., Jr. (2001). Function of *Escherichia coli* biotin carboxylase requires catalytic activity of both subunits of the homodimer. *J. Biol. Chem.* **276**, 29864–29870.
- Jitrapakdee, S., and Wallace, J.C. (1999). Structure, function and regulation of pyruvate carboxylase. *Biochem. J.* **340**, 1–16.
- Jitrapakdee, S., Vidal-Puig, A., and Wallace, J.C. (2006). Anaplerotic roles of pyruvate carboxylase in mammalian tissues. *Cell. Mol. Life Sci.* **63**, 843–854.
- Jitrapakdee, S., Adina-Zada, A., Besant, P.G., Surinya, K.H., Cleland, W.W., Wallace, J.C., and Attwood, P.V. (2007). Differential regulation of the yeast isozymes of pyruvate carboxylase and the locus of action of acetyl CoA. *Int. J. Biochem. Cell Biol.* **39**, 1211–1223.
- Jitrapakdee, S., St. Maurice, M., Rayment, I., Cleland, W.W., Wallace, J.C., and Attwood, P.V. (2008). Structure, mechanism and regulation of pyruvate carboxylase. *Biochem. J.* **413**, 369–387.
- Jogl, G., Tao, X., Xu, Y., and Tong, L. (2001). COMO: A program for combined molecular replacement. *Acta Crystallogr. D Biol. Crystallogr.* **57**, 1127–1134.
- Jones, T.A., Zou, J.Y., Cowan, S.W., and Kjeldgaard, M. (1991). Improved methods for building protein models in electron density maps and the location of errors in these models. *Acta Crystallogr. A* **47**, 110–119.
- Kondo, S., Nakajima, Y., Sugio, S., Yong-Biao, J., Sueda, S., and Kondo, H. (2004). Structure of the biotin carboxylase subunit of pyruvate carboxylase from *Aquifex aeolicus* at 2.2 Å resolution. *Acta Crystallogr. D Biol. Crystallogr.* **60**, 486–492.
- Mochalkin, I., Miller, J.R., Evdokimov, A., Lightle, S., Yan, C., Stover, C.K., and Waldrop, G.L. (2008). Structural evidence for substrate-induced synergism and half-sites reactivity in biotin carboxylase. *Protein Sci.* **17**, 1706–1718.
- Modak, H.V., and Kelly, D.J. (1995). Acetyl-CoA-dependent pyruvate carboxylase from the photosynthetic bacterium *Rhodobacter capsulatus*: rapid and efficient purification using dye-ligand affinity chromatography. *Microbiology* **141**, 2619–2628.
- Murshudov, G.N., Vagin, A.A., and Dodson, E.J. (1997). Refinement of macromolecular structures by the maximum-likelihood method. *Acta Crystallogr. D Biol. Crystallogr.* **53**, 240–255.
- Otwinowski, Z., and Minor, W. (1997). Processing of X-ray diffraction data collected in oscillation mode. *Methods Enzymol.* **276**, 307–326.
- Pettersen, E.F., Goddard, T.D., Huang, C.C., Couch, G.S., Greenblatt, D.M., Meng, E.C., and Ferrin, T.E. (2004). UCSF Chimera—a visualization system for exploratory research and analysis. *J. Comput. Chem.* **25**, 1605–1612.
- Robinson, B.H. (2006). Lactic acidemia and mitochondrial disease. *Mol. Genet. Metab.* **89**, 3–13.
- Rosenthal, P.B., and Henderson, R. (2003). Optimal determination of particle orientation, absolute hand, and contrast loss in single-particle electron cryomicroscopy. *J. Mol. Biol.* **333**, 721–745.
- Shen, Y., Chou, C.-Y., Chang, G.-G., and Tong, L. (2006). Is dimerization required for the catalytic activity of bacterial biotin carboxylase? *Mol. Cell* **22**, 807–818.
- St. Maurice, M., Reinhardt, L., Surinya, K.H., Attwood, P.V., Wallace, J.C., Cleland, W.W., and Rayment, I. (2007). Domain architecture of pyruvate carboxylase, a biotin-dependent multifunctional enzyme. *Science* **317**, 1076–1079.
- Studer, R., Dahinden, P., Wang, W.-W., Auchli, Y., Li, X.-D., and Dimroth, P. (2007). Crystal structure of the carboxyltransferase domain of the oxaloacetate decarboxylase Na⁺ pump from *Vibrio cholerae*. *J. Mol. Biol.* **367**, 547–557.
- Sueda, S., Islam, M.N., and Kondo, H. (2004). Protein engineering of pyruvate carboxylase. Investigation on the function of acetyl-CoA and the quaternary structure. *Eur. J. Biochem.* **271**, 1391–1400.
- Tong, L. (2005). Acetyl-coenzyme A carboxylase: crucial metabolic enzyme and attractive target for drug discovery. *Cell. Mol. Life Sci.* **62**, 1784–1803.
- Wallace, J.C., Jitrapakdee, S., and Chapman-Smith, A. (1998). Pyruvate carboxylase. *Int. J. Biochem. Cell Biol.* **30**, 1–5.
- Wexler, I.D., Kerr, D.S., Du, Y., Kaung, M.M., Stephenson, W., Lusk, M.M., Wappner, R.S., and Higgins, J.J. (1998). Molecular characterization of pyruvate carboxylase deficiency in two consanguineous families. *Pediatr. Res.* **43**, 579–584.
- Xiang, S., and Tong, L. (2008). Crystal structures of human and *Staphylococcus aureus* pyruvate carboxylase and molecular insights into the carboxyl-transfer reaction. *Nat. Struct. Mol. Biol.* **15**, 295–302.
- Yong-Biao, J., Islam, M.N., Sueda, S., and Kondo, H. (2004). Identification of the catalytic residues involved in the carboxyl transfer of pyruvate carboxylase. *Biochemistry* **43**, 5912–5920.